Research Article | Vol. 29, No. 15 / 19 July 2021 / Optics Express 23447
Optics EXPRESS

Optimization of frequency combs spectral-flatness using evolutionary algorithm

THYAGO PINTO,[1,*] UIARA C. DE MOURA,[1] FRANCESCO DA ROS,[1] MARKO KRSTIĆ,[2] JASNA V. CRNJANSKI,[2] ANTONIO NAPOLI,[3] DEJAN M. GVOZDIĆ,[2] AND DARKO ZIBAR[1]

[1]*DTU Fotonik, Department of Photonics Engineering, Technical University of Denmark, Kgs. Lyngby, Denmark*
[2]*School of Electrical Engineering, University of Belgrade, Belgrade, Serbia*
[3]*Infinera, London, UK*
[*]*thypi@fotonik.dtu.dk*

Abstract: We demonstrate the use of meta-heuristics algorithms for flatness optimization of optical frequency combs (OFCs). Without any additional component for flatness compensation, the laser alone is explored when driven by optimized bias current and radio frequency (RF) driving signals composed by multiple harmonics. The bias current amplitude and RF harmonic amplitudes and relative phases are optimized using particle swarm optimization (PSO) and differential evolution (DE) algorithms. The numerical results lead to a 9 lines-GS-laser-based OFC spectrum with 2.9 dB flatness. An online experimental optimization using the DE algorithm results in a 7-line-GS-laser-based OFC with 2 dB flatness.

1. Introduction

The current increase of data traffic in optical networks has encouraged the use of optical frequency combs (OFC) in Nyquist-dense-wavelength division multiplexing (N-DWDM) [1,2], orthogonal frequency division multiplexing (OFDM) [3], and comb-based super-channel systems [4]. This is motivated by the OFCs capacity of offering multiple optical carries, spaced within a fixed bandwidth and with a defined power distribution [5]. Most popular alternatives to generate OFCs are mode-locked semiconductor lasers (MLL) [6], four-wave mixing (FWM) [7], external electro-optical modulators (EOM) [8,9], and gain-switching (GS) lasers [10]. Due to their higher tunability and simple design, EOM and GS laser combs constitute good candidates for future optical communication systems [11]. In terms of power-efficient OFC generation, GS lasers stand out in comparison to EOM by requiring lower amplitude radio frequency (RF) signals [10].

Important OFC features are the carrier-to-noise ratio (CNR), the number of lines, and particularly the maximum to minimum peak power difference within a limited number of lines, referred to as flatness [3,12]. To increase the number of carriers inside a targeted flatness, the combination of lasers with Mach-Zehnder modulators (MZMs), phase modulator (PM), and dual-drive MZM (DD-MZM) is commonly explored [13,14]. Alternatively, harmonic superposition over the modulators driving signals can improve the OFC performance [15,16]. To avoid manual adjustments of the lasers and modulators driving signals, recent works have demonstrated the use of metaheuristics procedures, such as differential evolution (DE) algorithms, to shape the spectrum of MZM-based OFCs. In [14,17], an offline optimization approach is presented and the optimal modulators driving signals are achieved based on numerical models before have been applied in the experimental setup.

The use of modulator-based OFCs leaves unexplored the potential of the laser alone in producing a high-performance OFC. The laser-based OFC performance can be improved by driving the device with an RF signal composed of multiple harmonics and an optimized tailored driving signal. In this setup, the degrees of freedom are the amplitudes and relative phases of the

#430402 https://doi.org/10.1364/OE.430402
Journal © 2021 Received 2 May 2021; revised 1 Jul 2021; accepted 1 Jul 2021; published 9 Jul 2021

Optics EXPRESS

harmonics composing the RF signal and the bias current. This is a complex optimization where the goal is to find the driving signal characteristics that lead to a target OFC performance [18] in terms of CNR, number of lines, and flatness. Manually fine-tuning the driving signal features is time-consuming and may not provide an optimal solution for a high number of adjustable parameters.

In this work, we propose a GS-laser-based OFCs generation using optimized bias and an RF driving signal composed of multiple harmonics. The multiple harmonics RF driving signal is applied directly to the laser, simplifying the OFC setup as modulators are not present in the structure. The bias current and the amplitudes and relative phases of the RF harmonics are optimized online by means of gradient-free optimizers [19,20]. Particle swarm optimization (PSO) and DE algorithms are applied to a GS-laser-based OFC numerical model leading to an optimized OFC with 9 lines and 2.9 dB and 3.3 dB flatness for the DE and PSO optimizers, respectively. Additionally, an online experimental proof-of-concept is demonstrated. By driving a directly modulated laser (DML) with an RF signal and bias optimized by the DE algorithm, an optimal spectrum with 7 lines and 2 dB flatness is obtained. Thanks to the use of gradient-free methods, these optimizations are performed online and without previous/posterior processing of the data. Moreover, for the laser utilized in the experiment, the optimization is carried out without the need for a defined model. The metaheuristics algorithms are attractive alternatives for optimizing device responses whose models are unknown or non-differentiable.

This article is organized as follows. In Section 2., the model for generating OFCs based on GS lasers and the harmonic superposition utilized as driving signals are mathematically described. In Section 3., the PSO and DE algorithms are detailed with a focus on OFC flatness optimization. In Section 4., results based on the GS-laser numerical model are evaluated using PSO and DE algorithms. A proof-of-concept experimental demo is presented in Section 5., firstly describing the experimental setup and then applying the DE algorithm in an online experimental optimization of the flatness of a DML-based OFC. Section 6 summarizes the contributions of using harmonic superposition for the driving signals of GS laser-based OFCs combined with a gradient-free online optimization methodology.

2. Optical frequency combs based on the gain switching laser model

An OFC is a sequence of optical carriers (or lines) equally spaced in the spectrum by a modulation frequency. A simple and efficient method for OFC generation is the use of a GS laser driven by an electrical signal $I(t)$. The great advantage of this technique is the tunability as the space between the OFC lines can be adjusted by changing the fundamental frequency of the driving signal $I(t)$. In the numerical analysis of this work, a multiple quantum well-distributed feedback laser (DFB) in GS mode is utilized. In order to describe the laser dynamics more realistically, we employ an extended rate equation model of the laser [21,22], including carrier transport and parasitic effects, governing the dynamics of the carrier density in the barrier n_b, the carrier density in the well regions n_w, the photon density S, and the optical phase θ as in

$$\frac{dn_b}{dt} = \frac{n_{\text{inj}} I}{qV_{\text{tot}}} - \frac{n_b}{\tau_b} - \frac{n_b}{\tau_{bw}} + \frac{n_w V_w}{\tau_{wb} V_{\text{tot}}}, \tag{1}$$

$$\frac{dn_w}{dt} = \frac{n_b V_{\text{tot}}}{\tau_{bw} V_w} - \frac{n_w}{\tau_w} - \frac{n_w}{\tau_{wb}} - \frac{v_g \Omega (n_w - n_0) S}{1 + \epsilon S}, \tag{2}$$

$$\frac{dS}{dt} = \frac{\Gamma v_g \Omega (n_w - n_0) S}{1 + \epsilon S} - \frac{S}{\tau_p} + \frac{\Gamma R_{sp}}{V_{\text{tot}}}, \tag{3}$$

$$\frac{d\theta}{dt} = \frac{1}{2} \alpha \Gamma v_g \Omega (n_w - n_{th}), \tag{4}$$

where n_{inj} is the injection efficiency, V_{tot} is the total volume of the separate confinement heterostructure (SCH) and the active region, V_w represents the volume of the wells, τ_w, and τ_b

Optics EXPRESS

are the carrier lifetimes in the well and in the barrier regions, respectively, τ_{bw} is the capture time, τ_{wb} stands for the escape time, Ω is the differential gain, τ_p means the photon lifetime, ϵ is the nonlinear gain suppression coefficient, Γ stands for the optical confinement factor, n_0 is the carrier transparency density, R_{sp} is the spontaneous emission rate, α is the linewidth enhancement factor, q is the electron charge and v_g represents the group velocity.

The laser driving current $I(t)$ is composed of a bias (direct) current c_0 and a sinusoidal part. For a single harmonic RF driving signal, the sinusoidal part is represented by $c\sin(2\pi f_0 t)$ with f_0 being the fundamental frequency and c the driving signal amplitude. The frequency f_0 determines the space between the OFC lines.

In this work, the potential capability of the laser alone, i.e., without any modulator in the setup, is explored to improve the OFC characteristics. For that, multiple harmonics are considered in $I(t)$. The multiple harmonic driving signal provides more flexibility in terms of tailoring $I(t)$ to accomplish targeted features in the OFC profile. This is potentialized by the use of gradient-free optimizers to allow high-quality OFC in terms of flatness, the number of carriers, and CNR. Therefore, the laser driving signal is described as

$$I(t) = c_0 + \sum_{h=1}^{N} |c_h| \sin(2\pi h f_0 t + \phi_h), \tag{5}$$

where N stands for the number of harmonics, c_0 is the constant bias amplitude, and c_h and ϕ_h are the amplitude and phase of the harmonics in the driving signal, respectively.

At the laser output, by solving Eqs. (1)–(4), the complex electric field E_{GS} is achieved by [10]

$$E_{\mathrm{GS}}(t) = \sqrt{S(t)}\exp\left(j\theta(t)\right). \tag{6}$$

The OFC flatness for the model in Eqs. (1)–(4) is determined in the frequency domain by applying the Fourier transform over $E_{\mathrm{GS}}(t)$. The flatness is calculated in the resulting spectrum as aforementioned.

3. Gradient-free optimization framework for OFC spectral flatness

3.1. Problem formulation

The laser-based OFC spectral flatness depends on the driving signal features applied to the laser and shown in Eq. (5). These features are the amplitudes of the bias current c_0, the amplitudes c_h, and the phases ϕ_h of the harmonics. In this work, the relative phases composing the laser RF driving signal are considered. The relative phases between harmonics v and z are represented by $\Delta\phi_{v,z}$. Moreover, manipulating c_0, N, c_h and $\Delta\phi_{v,z}$ has an impact not only over the OFC flatness but over the maximum OFC launched power, the number of generated carriers within a certain flatness and the CNR. Optimizing the features in Eq. (5) means extracting the best operation points of the OFC setup and improve the overall characteristics of the system where the OFC is applied. Manually fine-tuning the parameters of Eq. (5) is cumbersome and may lead to not optimal solutions as N increases. Thus we propose an OFC optimization method using gradient-free algorithms such as PSO and DE. For this end, we call a solution candidate $\mathbf{x}$ the vector of parameters present in Eq. (5) and to be optimized online using the DE and PSO algorithms. For N harmonics, the solution candidate is described as

$$\mathbf{x} = [c_0\ c_1\ c_2\ \cdots\ c_N\ \Delta\phi_{1,N}\ \Delta\phi_{2,N}\ \cdots \Delta\phi_{N-1,N}]. \tag{7}$$

The OFC optimization depends on the target characteristics in the resulting spectrum. In our case, the target is to minimize the flatness of a defined number of OFC lines. In this context, the DE and PSO algorithms use a fitness function $f(\cdot)$, which evaluates the spectra produced by

Optics EXPRESS

each solution candidate $\mathbf{x}$ when applied to the laser. The final optimized solution is obtained by iteratively minimizing $f(\cdot)$ as it will be described in detail for each algorithm in Sections 3.2 and 3.3. For both DE and PSO, the cost function $f(\cdot)$ is the variance of the vector containing the peak power values of L consecutive carriers in the OFC as in $\mathbf{P} = [P_1\ P_2\ \cdots\ P_L]$. $\mathbf{P}$ is generated by the solution $\mathbf{x}$ when applied to the laser. Mathematically, the fitness function is described as

$$f(\mathbf{x}) = \frac{1}{L-1}\sum_{l=1}^{L}|P_l - \mu|^2, \tag{8}$$

where μ is the mean of $\mathbf{P}$ as $\mu = \frac{1}{L}\sum_{l=1}^{L} P_l$.

The main advantage of using gradient-free approaches is that the optimization is performed online directly on the laser and the resulting OFC spectrum. Derivative-free algorithms are particularly useful for problems when the model is not explicitly available, as it is the case for the laser utilized in the experimental part of this work.

3.2. Particle swarm optimization algorithm for OFC optimization

The PSO is a population-based stochastic algorithm in which a set of N_p particles moves in a limited solution space. In the case of OFCs optimization shown in this work, the particles correspond to the solution candidates $\mathbf{x}$ as defined in Eq. (7) and the solution space correspond to the limits of each element inside $\mathbf{x}$. The range of values for each component in $\mathbf{x}$ is mainly defined by the operational limits of the laser utilized in the model or the experimental setup. At each iteration, the particle movement is evaluated based on its corresponding OFC spectral response. The OFC response is quantified using the cost function $f(\mathbf{x})$ defined in Eq. (8). The overall optimization goal is to minimize $f(\mathbf{x})$ and, therefore, to generate a highly flat OFC spectrum. At the instant (iteration) k, the position of each particle i is updated using a search-grid method based on [19]

$$\mathbf{x}_{k,i} = \mathbf{x}_{k-1,i} + \mathbf{v}_{k,i}, \tag{9}$$

where $\mathbf{x}_{k,i}$ and $\mathbf{v}_{k,i}$ represent the position and velocity of the particle, respectively. For individual solutions, the searching movement inside the grid is also influenced by other particles [23], and $\mathbf{v}_{k,i}$ takes into consideration the best group movement decision $\mathbf{g}_{\text{best}}$, i.e., the solution that produces the best OFC flatness until the previous iteration, as in

$$\begin{aligned}\mathbf{v}_{k,i} = w\cdot\mathbf{v}_{k-1,i} &+ c_{a1}\cdot r_{\text{PSO1}}(\mathbf{p}_{\text{best},i} - \mathbf{x}_{k-1,i})\\ &+ c_{a2}\cdot r_{\text{PSO2}}\cdot(\mathbf{g}_{\text{best}} - \mathbf{x}_{k-1,i}),\end{aligned} \tag{10}$$

with $\mathbf{p}_{\text{best},i}$ being the best solution found by the particle i, w representing the inertia, $\mathbf{g}_{\text{best}}$ is the best general solution (best OFC flatness) found so far considering all vectors. The acceleration coefficients c_{a1} and c_{a2} are generally equal to 1, while r_{PSO1} and r_{PSO2}, the exploration and exploitation parameters, respectively, vary between 0 and 1. These four last parameters scale the contribution of the cognitive and individual movement and the social component towards the solution [24]. They are adjusted to the OFC flatness optimization problem as their values highly impact the convergence of the algorithm to an optimal solution. The structure of the PSO OFC flatness optimization is shown in Algorithm 1, for the number of iterations N_{ite}.

Optics EXPRESS

Algorithm 1: OFC PSO Pseudo-Code

```
Initialize positions x_{0,i} and velocities v_{0,i};
Find best initial solution g_best by f(x_{0,i});
while k less than N_ite do
    for i = 1 to N_p particles do
        Calculate v_{k,i} with Eq. (??);
        Update x_{k,i} with Eq. (??);
        Check laser driving signal limits;
        Apply the solution to the laser;
        Evaluate the OFC flatness by
         f(x_{k,i});
        if f(x_{k,i}) < f(p_{best,i}) then
            p_{best,i} = x_{k,i} ;
        end
        if f(x_{k,i}) < f(g_best) then
            g_best = x_{k,i};
        end
    end
end
```

Algorithm 2: OFC DE Pseudo-Code

```
Initialize solutions X_{0,i};
Find best initial solution g_best by f(X_{0,i});
while k less than N_ite do
    for i = 1 to N_c do
        Generate v_{k,i} with Eq. (??);
        Generate u_{k,i} with Eq. (??);
        Check laser driving signal limits;
        Apply the solution to the laser;
        Evaluate the OFC flatness by
         f(u_{k,i});
        if f(u_{k,i}) < f(x_{k,i}) then
            x_{k+1,i} = u_{k,i};
        end
        if f(u_{k,i}) < f(g_best) then
            g_best = u_{k,i};
        end
    end
end
```

3.3. Differential evolution algorithm for OFC optimization

The DE algorithm uses genetic algorithm concepts and it is a derivative-free, population-based and memoryless class of optimization method [20]. It has three stages: mutation, crossover, and fitness evaluation. For the OFC flatness optimization, initially at iteration $k = 0$, a population is generated with N_c solution candidates $\mathbf{x}$ as defined in Eq. (7). This initial population $\mathbf{X}_{k=0} = \{\mathbf{x}_{0,1}, \mathbf{x}_{0,i}, \ldots, \mathbf{x}_{0,N_c}\}$ contains values uniformly distributed between the laser operational limits of the individual components within $\mathbf{x}$, where k represents the iteration and i the solution between 1 and N_c. For the following $k \geq 0$ iterations, the mutation creates a donor vector $\mathbf{v}_{k,i}$ by mixing random solutions in the current population $\mathbf{x}_{k,1:N_c}$. In this work, each $\mathbf{v}_{k,i}$ is calculated as

$$\mathbf{v}_{k,i} = \mathbf{x}_{k,r_1} + F \cdot (\mathbf{x}_{k,r_2} - \mathbf{x}_{k,r_3}), \quad i = 1, \ldots, N_c, \tag{11}$$

where r_1, r_2 and r_3 are randomly generated population indexes $\in \{1, 2, \ldots, N_c\}$, and F is a scaling factor within [0:1]. Next, the crossover generates the trial vector $\mathbf{u}_{k,i}$, which mixes $\mathbf{v}_{k,i}$ and $\mathbf{x}_{k,i}$. Notice that $\mathbf{v}_{k,i}$, $\mathbf{x}_{k,i}$ and $\mathbf{u}_{k,i}$ are OFC combs driving signals and solution candidates as defined in Eq. (7). Therefore, each element d in $\mathbf{u}_{k,i}$ is a driving current parameter (amplitude or relative phase) that is generated as a binomial crossover as in

$$u_{k,i,d} = \begin{cases} v_{k,i,d}, & \text{if } r_c \leq p_c, \\ x_{k,i,d}, & \text{if } r_c > p_c, \end{cases} \tag{12}$$

where p_c is the probability of crossover and r_c is a random number between 0 and 1 generated per element d. Before applying it to the laser, the boundaries of $\mathbf{u}_{k,i}$ are checked to avoid values outside the physical limits of the laser. Finally, in the fitness evaluation step, the OFC spectral response of driving the laser with $\mathbf{u}_{k,i}$ is verified according to Eq. (8). The solution candidate is updated, if the OFC flatness performance provided by $f(\mathbf{u}_{k,i})$ is better than the current solution $f(\mathbf{x}_{k,i})$

$$\mathbf{x}_{k+1,i} = \begin{cases} \mathbf{u}_{k,i}, & \text{if } f(\mathbf{u}_{k,i}) < f(\mathbf{x}_{k,i}) \\ \mathbf{x}_{k,i}, & \text{otherwise.} \end{cases} \tag{13}$$

Optics EXPRESS

The overall best flatness OFC response found by all solution candidates is updated in a similar manner as in

$$\mathbf{g}_{\text{best}} = \mathbf{u}_{k,i}, \text{ if } f(\mathbf{u}_{k,i}) < f(\mathbf{g}_{\text{best}}). \tag{14}$$

The procedure to apply DE optimization over the OFC flatness is synthesized in Algorithm 2, for the number of iterations N_{ite}.

4. Numerical analysis

4.1. DE and PSO OFC flatness optimization

In the numerical analysis, the OFCs are generated using the GS-laser model described in Section 2. The laser parameters considered in Eqs. (1)–(4) are specified in Table 1. For each solution and iteration, the gradient-free OFC flatness optimization using DE and PSO algorithms is implemented in the setup shown in Fig. 1. The impact over the number of lines and flatness of the OFC is evaluated by driving the laser with a signal composed by one ($N = 1$) or three ($N = 3$) harmonics and assuming $f_0 = 5$ GHz in Eq. (5). For $N = 1$, the solution candidates in Eq. (7) are defined by $\mathbf{x} = [c_0\ c_1]$ and for $N = 3$, $\mathbf{x} = [c_0\ c_1\ c_2\ c_3\ \Delta\phi_{1,3}\ \Delta\phi_{2,3}]$. The algorithms' searching space is defined by limiting c_h within [25:80] mA with $h \in \{0, 1, 2, 3\}$ and $\Delta\phi_{1,3}$ and $\Delta\phi_{2,3}$ between 0 and 2π. For $N = 3$, the phase reference is in the first harmonic.

In Fig. 1, at each iteration, each solution candidate $\mathbf{x}$ provides the driving signal features of Eq. (5) to be applied to the DFB laser model. At the laser output, the spectrum of the complex electric field is calculated using a fast Fourier transform (FFT), followed by a logarithm scale, a normalization, and the extraction of the peak power values in a specific OFC spectrum window which includes the maximum power. The OFC peak powers are found using a find peaks function. The peak powers are allocated in the vector $\mathbf{P}$. The vector $\mathbf{P}$ is delivered to the DE or PSO algorithms and evaluated by the fitness function of Eq. (8) in terms of flatness. This methodology follows for all the solutions i between 1 and $N_c = N_p$ and for all iterations k between 1 and the maximum number of iterations N_{ite} as presented in Algorithms 1 and 2.

The DE algorithm considers the population size $N_c = 40$, the scaling factor $F = 0.6$, probability of crossover $p_c = 0.8$. In the PSO, $N_p = 40$ is the number of particles while, $w = 0.7213$, $r_{\text{PSO1}} = 1.1931 \times G_1$, $r_{\text{PSO2}} = 1.1931 \times G_2$, where G_1 and G_2 are random values between 0 and 1 and with $G_1 + G_2 = 1$. A decrease in the best solution OFC flatness response is performed progressively until $N_{ite} = 100$ for both optimizers.

Figure 2 shows the optimized OFCs when applying to the laser the final best solution found by the DE and PSO algorithms. These results constitute the best OFCs spectra achieved in terms of combined flatness and the number of lines for the presented DFB laser model. For $N = 3$,

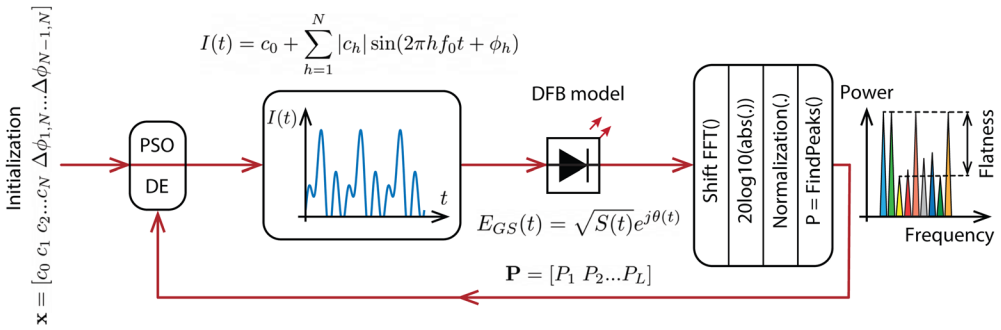

Fig. 1. OFC numerical setup per solution/iteration for flatness optimization using PSO or DE algorithms. DFB: Distributed feedback Laser. FFT: Fast Fourier transform. PSO: Particle swarm optimization. DE: Differential evolution.

Optics EXPRESS

Table 1. Parameters for the Laser Model of Eqs. (1)–(4)

Parameter	Value
Injection efficiency (n_{inj})	0.85
Total volume of the SCH (V_{tot})	$1.03 \cdot 10^{-10}\text{cm}^3$
Volume of the well (V_w)	$1.68 \cdot 10^{-11}\text{cm}^3$
Carrier lifetimes in the well (τ_w)	1.5 ns
Carrier lifetimes in the barrier (τ_b)	2.5 ns
Capture time (τ_{bw})	14.5 ps
Escape time (τ_{wb})	70 ps
Differential gain (Ω)	$1.5 \cdot 10^{-15}\text{cm}^2$
Photon lifetime (τ_p)	2.3 ps
Nonlinear gain suppression coefficient (ϵ)	$2 \cdot 10^{-17}\text{cm}^4$
Optical confinement factor (Γ)	0.08
Carrier transparency density (n_0)	$4.2 \cdot 10^{18}\text{cm}^{-3}$
Spontaneous emission rate (R_{sp})	$1.2 \cdot 10^{12}\text{s}^{-1}$
Linewidth enhancement factor (α)	3.5
Electron charge (q)	$1.6 \cdot 10^{-19}$ C
Group velocity (v_g)	$8.5 \cdot 10^9$ cm/s

a 9-lines OFC is achieved with 2.9 dB and 3.3 dB flatness for the DE and PSO algorithms, respectively. With fewer parameters and less complex manual optimization, the DE OFC flatness optimization for the single harmonic laser driving signal is shown in Fig. 2(c). The combined harmonic superposition provides 2.8 dB and 2.4 dB OFC flatness gain, for the DE and PSO cases, respectively, when compared with the single harmonic case. The PSO case is not presented for $N = 1$ due to similar results as for the DE case. These results confirm the benefits to the OFC flatness of applying harmonic superposition to the laser driving signal when combined with an optimization algorithm.

The features of the driving signal of the optimized combs are presented in Table 2 and the respective current waveforms in Fig. 2(d). For $N = 3$, the different amplitudes and relative phases found by DE and PSO algorithms lead to different driving current shapes, but with close OFC performance in terms of flatness. Furthermore, as presented in Fig. 2(e), the algorithms converge to close fitness as in their final solutions when near 40 iterations, although the DE continues slightly improving the minimum variance towards the end of 100 iterations (generations). The resulting OFCs provide a good compromise between minimum flatness and the maximum number of lines L. The DE and PSO algorithms belong to the same class of optimization methods, making reasonable similar results under the same constraints. Alternatively, the methodology can be applied to targeted values of OFC peak power values by simply altering the fitness function to incorporate the desired spectrum profile.

Table 2. OFC Optimized Driving Signal Features Solutions $\mathbf{x}$ and Obtained Performance (Number of Lines $\mathbf{L}$ and Flatness) Found Using PSO and DE Algorithms Related to Fig. 2

	$\mathbf{x} = [c_0\ c_1\ c_2\ c_3\ \Delta\phi_{1,3}\ \Delta\phi_{2,3}]$	Flatness	$\mathbf{L}$
	[mA mA mA mA rad rad)	(dB)	
DE	[25.2 20.0 20.0 24.9 5.70 3.56]	2.9	9
PSO	[32.1 29.8 26.4 25.3 0.62 0.7]	3.3	9
DE	[25.0 26.0 - - - -]	5.7	9

Optics EXPRESS

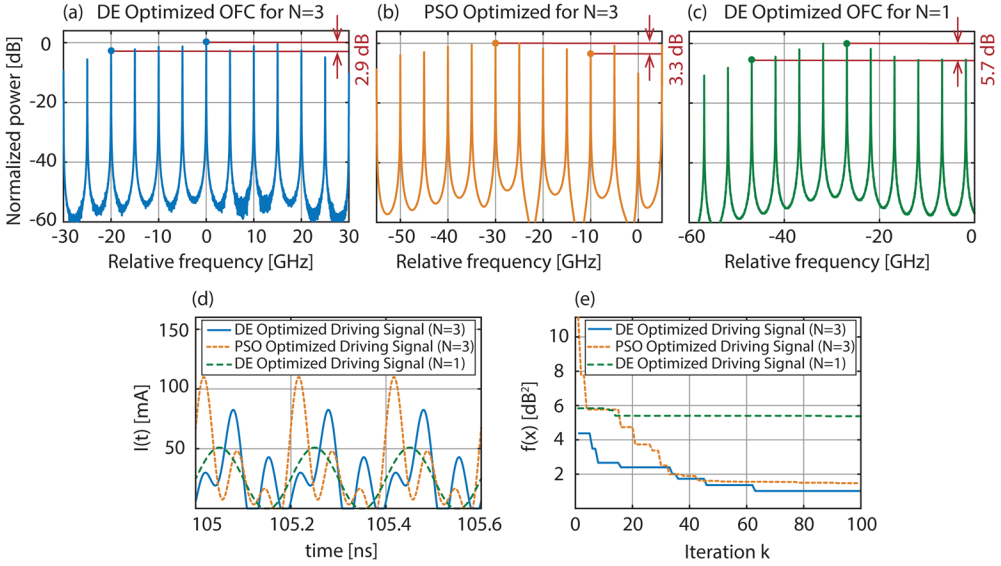

Fig. 2. Optimized GS-laser OFCs results for single harmonic laser driving signal ($N = 1$) and multiple harmonics laser driving signal ($N = 3$).

In achieving OFCs with narrower flatness using the model, the major limitations come from the number of harmonics in the laser driving signal, the laser modulation bandwidth, its linewidth enhancement factor, and the optimization constraints over the OFC frequency window around the maximum power and minimum bias current.

5. Experimental analysis

5.1. Setup

A proof-of-concept experimental demo setup for OFC flatness optimization is shown in Fig. 3. The single harmonic ($N = 1$) and three harmonics ($N = 3$) cases are considered for the laser driving signal of Eq. (5). The multi harmonics laser driving signal is achieved using the signal generators (SGs) Anritsu MG3694C, Agilent E8267D, and Agilent E8247C with frequencies in 5 GHz, 10 GHz, and 15 GHz, respectively. Their outputs are combined using two couplers

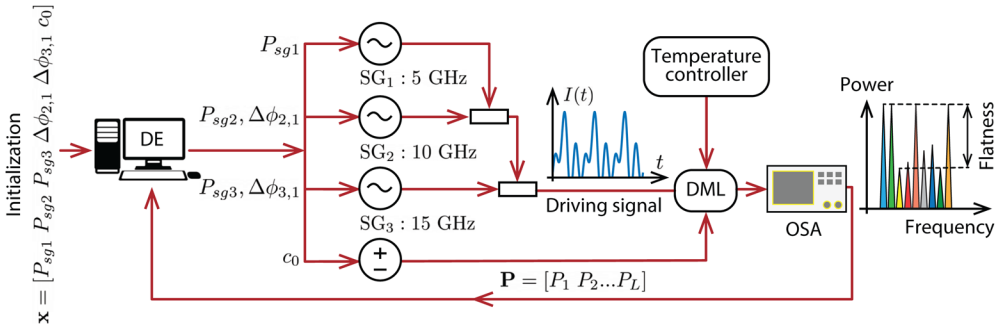

Fig. 3. OFC setup of the online optimization using DE Algorithm. SG: Signal Generator. OSA: Optical Spectrum Analyzer. P_{SG}: Power Signal Generator [dBm]. c_0: Bias current [mA], $\Delta\phi_{v,z}$: relative phase between SGs v and z.

Optics EXPRESS

with 6 dB loss each. Moreover, for $N = 3$, the SGs clocks are synchronized. The resulting RF signal drives a DML (NLK1551SSC), while the bias current is provided by an Agilent E3646A power supply. The laser minimum value for the high cutoff frequency is 14 GHz. The laser temperature is controlled by the ThorLabs TED 200 with a resistance set to 10 kΩ. The temperature controller is maintained in the same value along the experiment. The OFC is captured using a high-resolution optical spectrum analyzer (OSA) Finisar WaveAnalyzer 1500s, and its performance is optimized by the gradient-free algorithm which controls the SGs and power supply outputs. It must be stressed that the DML laser utilized in the experimental setup and the DFB model described in Section 2 are independent, i.e., the parameters given in Table 1 are fitted to the Gooch & Housego AA0701 series DFB laser used in [10]. The experiment corresponds to a proof-of-concept of the exposed method.

Since the PSO and DE algorithms presented close performances in the numerical analysis and, to evaluate several cases for different values of L, the DE is the only algorithm utilized throughout the experimental validation. The procedure considered in the following sections can be applied replacing the DE for the PSO algorithm without significant changes or loss of performance. The DE algorithm considers $N_c = 30$ solution candidates $\mathbf{x}$ per iteration, the scaling factor $F = 0.6$, probability of crossover $p_c = 0.8$, boundaries limited by the operational limits of the laser, and the fitness function as in Eq. (8). The parameters values p_c and F are manually optimized to improve the convergence process. After combining the three harmonics, the total RF power is restricted to 12 dBm for the optimization process to avoid damaging the laser. The maximum of $L = 9$ is considered since for 8 lines the results already led to flatness above 3 dB.

Additionally to the constraints regarding the maximum value of RF power at the laser input, the minimum bias current boundary is limited beyond its threshold value. The reason is to avoid solutions leading to an OFC spectrum with CNR inferior to 20 dB as presented in Fig. 4(a), observable for lower values of bias current. The spectrum in Fig. 4(a) is the result of driving the laser with a bias current of 24.2 mA and an RF amplitude of 11.12 dBm. OFC spectra with low values of CNR tend to misguide the DE algorithm. Therefore, OFCs with a CNR of 20 dB are not desired in our design and are excluded from the optimization. This is carried out by limiting the bias current within [25:120] mA for one harmonic optimization and [35:120] mA for three, and consequently beyond the laser threshold current of 15 mA. A requirement over the maximum power in at least one of the OFC lines is established in −20 dBm and to maximize the launched power in the lines. The constrain over the CNR is optional and the goal is to achieve a high-quality OFC with high CNR throughout the optimization. Low values of CNR tend to lead to distorted and noisy spectra and impact the performance of the OFC application in an end-to-end transmission.

Figure 4(b) presents the stability analysis of the laser. It shows the variation in the peak power of the DML generated spectrum when the laser is driven only by the bias current varying from 20 mA to 100 mA. The DML considered possesses a certain degree of amplitude noise over the peak power measured in the central line as the bias current is increased. This variation impacts the OFC behavior as it tends to follow over the peak powers of the sideline carriers when using the laser for comb generation. To overcome the effect of these oscillations in the DE OFC flatness convergence optimization process, the evaluation of the OFC measured peak powers per line generated by each solution $\mathbf{x}$ is averaged over 5 consecutive measurements. Additionally, when a local minimum is found (best flatness), the OFC spectral response provided by the candidate is reevaluated with the average of 50 new measurements of the peak powers per line. The algorithm only considers the solution as a global best solution if the flatness of the new averaged OFC peak power per line measurements maintains a better performance than the current general optimal solution. As a compromise between accuracy and time demanded, 50 measurements is an appropriate value for the re-evaluation of a potential $\mathbf{g}_{\text{best}}$. The averaging of OFC measured spectra is performed to assess accurately the comb performance and mitigate

Optics EXPRESS

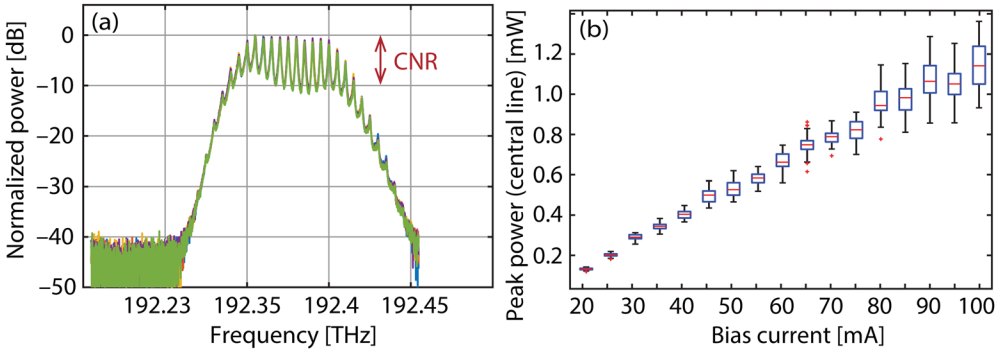

Fig. 4. Laser behavior (a) Example of an OFC with CNR inferior to 20 dB and to be excluded from the OFC flatness DE optimization (50 measured spectra overlapped). (b) Bias current variation and laser stability analysis of the peak power in the central line for 50 measurements.

the impacts of the amplitude noise over the optimization. Without averaging (capturing one single spectrum/solution candidate), the DE algorithm can assume the OFC response provided by a solution candidate leads to a low flatness when it mainly received as feedback a transient behavior. The OFC flatness fluctuations are in order of 1 dB. The averaging and the re-evaluation of solutions were able to eliminate disturbances in the algorithm convergence and provide reliable experimental validation of the proposed approach. Fluctuations in the amplitude and frequencies of the RF driving signals showed an inferior impact on the flatness of the comb than those presented by the bias.

In order to generate frequency combs with narrow flatness, the GS laser should operate in the nonlinear regime, in which the temporal forms of the output light intensity and phase follow distorted forms of the driving current. In this work, the control of the laser nonlinear response is achieved by gradient-free optimization, which provides an optimized form of the driving current pulse form.

5.2. Results

5.2.1. Amplitude optimization: one harmonic

First, the optimization is performed considering only one harmonic in the driving signal, at a frequency of 5 GHz (SG Anritsu MG3694C) and applied directly to the laser without passing through the couplers in Fig. 3. The solutions are defined as $\mathbf{x} = [c_0\ P_{SG1}]$, where P_{SG1} is the power of the SG. After 100 iterations, the DE algorithm finds the optimized solution presented in Table 3 as case 1. Driving the laser with these values and measuring 50 spectra with a 1-second interval between points, the average achieved flatness is 7.1 dB for 5 lines as presented in Fig. 5(a). The results are similar to the best flatness from the manual optimization of the comb that provides a flatness of 7.3 dB for 5 lines and with $c_0 = 24$ mA and $P_{SG1} = 10.15$ dBm. Due to the physical behavior of the laser, these are expected values since they correspond to a high RF power (near the laser operational limit) and low bias (near the threshold). Although the numerical model of Section 2 and the laser in the experiment are not related, they share the tendency of smaller flatness for lower bias current. When considering the constraints over the CNR, a different value of flatness is obtained in the experimental setup for a similar bias amplitude and RF signal as in the numerical results. A better flatness could be achieved at the cost of low CNR as reported in Fig. 4(a).

Optics EXPRESS

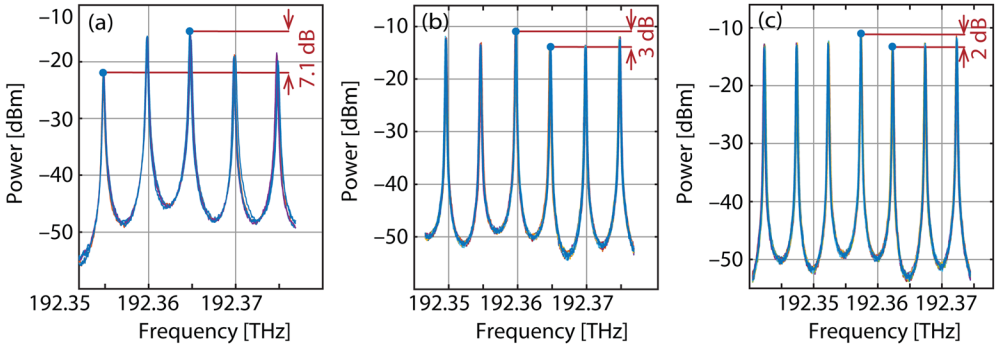

Fig. 5. Experimental OFC optimized (averaged flatness of 50 measured spectra overlapped) using DE algorithms for: (a) Case 1- one harmonic in the laser driving signal, (b) Case 3- three harmonic amplitudes of the laser driving signal, and (c) case 4 - three harmonic amplitudes and phases of the laser driving signal.

Table 3. Experimental Frequency Comb Optimization Solutions x and Performances When Applying DE Algorithm for Different Characteristics of the Driving Signal

Case	N	$\mathbf{x}$ =[c_0, P_{SG1}, P_{SG2}, P_{SG3}, $\Delta\phi_{2,1}$, $\Delta\phi_{3,1}$] [mA, dBm, dBm, dBm, rad, rad]	Flatness (dB)	L
1	1	[25.0, 12.0, -, -, -, -]	7.1	5
2	3	[39.0, 9.0, 7.4, −5.8, 0, 0]	5.1-7	7
3	3	[48.4, 7.7, 4.5, 4.8, 0, 0]	2.5-3.1	6
4	3	[1.4, 8.8, 4.5, 4.8, 1.9, 2.6]	2-2.3	7
5	3	[40.0, 7.9, 7.4, 1.6, 6.0, 6.3]	6.1	8
6	3	[56.7, 8.5, 7.4, 4.3, 6.1, 3.6]	6.2	9

5.2.2. Amplitude optimization: three harmonics

For 3 harmonics, the SGs launched powers vary from −5 dBm to 9 dBm, 7 dBm, and 5 dBm, for the first, second, and the third SG, respectively. This range is after the couplers and represents the power per harmonic at the input of the laser. An electrical amplifier is not present in the setup since it contributed to the harmonic distortion of the driving signal. This limited the launched power per harmonic below the laser operational limit. The difference between the maximum RF powers per harmonic consequently restricted the searching space when generating solutions $\mathbf{x} = [c_0\ P_{SG1}\ P_{SG2}\ P_{SG3}]$, where P_{SG2} and P_{SG3} are the power of the second and third SGs, respectively.

Different values for L in the cost function of Eq. (8) are evaluated throughout the DE optimization. The best flatness performance solution is obtained for $L = 6$ carriers at the point presented in Table 3 as case 3. For $L = 7$ as in case 2, the achieved flatness is higher than 5 dB while, for case 3, the solution leads to an OFC flatness of around 3 dB. The OFC obtained by using case 3 final solution is depicted in Fig. 5(b). Moreover, in case 3, the bias current is not close to the laser threshold value (15 mA) and the improvement in the flatness does not require a low bias current. The harmonics superposition allows targeting specific features in the spectral flatness of OFC, especially when combined with the DE optimization. Compared with the single harmonic case, the harmonic superposition proves 4 dB flatness gain and two extra carriers while maintaining a high CNR. The aforementioned limitation over the search space is expected to reduce the chances of finding more lines within 3 dB flatness. The search space is also limited

Optics EXPRESS

due to a minimum required peak power per line of the OFC to avoid values of the CNR inferior to 20 dB [18]. In the results, as presented in the DE algorithm optimized spectra of Fig. 5(b), a high-quality OFC with CNR around 40 dB is prioritized.

5.2.3. Amplitude and phase optimization: three harmonics

The DE algorithm is now used considering the amplitude and relative phases and Eq. (7) is readjusted as in $\mathbf{x} = [c_0\ P_{SG1}\ P_{SG2}\ P_{SG3}\ \Delta\phi_{2,1}\ \Delta\phi_{3,1}]$. The relative phase reference is established in the first harmonic. The best solution compromise for minimum flatness and maximum L is obtained for 2 dB OFC flatness over 7 lines as shown in Fig. 5(c) and case 4 shown in Table 3. Incorporating the relative phases into the solution candidates provides more flexibility and allows the DE optimization to achieve superior flatness by shaping the RF driving signal. This result constitutes the overall best operation point for the experimental optimization found throughout this work. For $L = 8$ and $L = 9$, an OFC flatness higher than 3 dB is achieved. The RF-launched power restrictions are expected to limit the improvement in performance in these cases. Even though, in comparison, they lead to better flatness than the single harmonic driving signal case. Cases 5 and 6 offer 3 or 4 extra lines, respectively, with at least 1 dB OFC flatness gain in comparison with case 1.

The convergence evolution is shown in Fig. 6. The algorithms can obtain good flatness values near 30 iterations and they keep improving the performance towards the end of the optimization. For example, it can be observed in Fig. 6 that an already good OFC flatness response in case 4 happened around the 30th iteration and the performance keeps improving towards the 100th iteration. This characteristic can be explored for faster optimization, depending on the target OFC. The long-term performance of the setup can be maintained in an interval of 1-2 hours with 1 dB OFC flatness and CNR fluctuations around the optimized values. A longer-term stability evaluation analysis was not part of the experiment and remains to be investigated in future works.

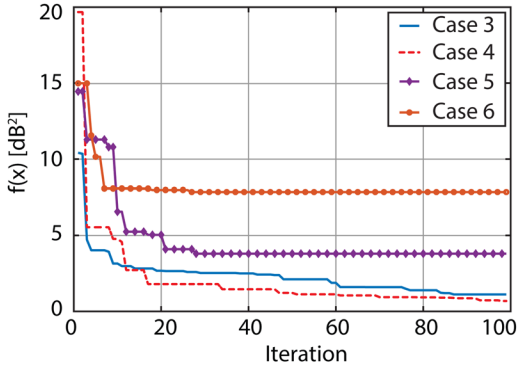

Fig. 6. OFC fitness convergence using DE Algorithm for the cases in Table 3

The optimization cases are performed online directly on the DML laser under test without any previous or posterior offline processing. In addition to operating conditions, the comb features depend on the laser characteristics. Consequently, different GS lasers may lead to different optimized inputs. However, the optimization method can be utilized regardless of the GS laser available.

There is a trade-off between the number of lines, comb spacing, and flatness. Due to the limited modulation bandwidth of GS laser, the increase of the comb spacing leads to the decrease of the number of lines or/and flatness since higher harmonics of the RF signal can not equally contribute to the GS laser output spectrum as lower. On the other hand, higher values of flatness increase the number of lines, since more lines with more unequal peak power values can fall into

Optics EXPRESS

a given flatness range. This means that performance of GS laser with respect to the number of lines, comb spacing, and flatness can not be considered independently, but rather in the context of other performance indicators and operating conditions.

In the experiment, the main limitation to achieve more comb lines within a narrow flatness is the laser modulation bandwidth, its linewidth enhancement factor, the number of harmonics in the laser driving signal as well as their corresponding amplitudes and relative phases. The constraints imposed by the optimization over the driving signals and the search space also contribute to a limited number of lines.

In principle, the number of comb lines and flatness can be improved by using a GS laser with higher modulation bandwidth, larger linewidth enhancement factor combined with driving current temporal form comprising higher harmonics with optimized amplitudes and relative phases. The number of harmonics is, in principle, limited by the laser modulation bandwidth. It means that it is possible to change comb spacing e.g., from 5 GHz to 10 GHz, which for a fixed modulation bandwidth of the GS laser leads to reduction of the available number of harmonics contributing to comb lines. For larger comb spacing it is recommended to use a laser with higher modulation bandwidth. It should be noted that an increase of alpha-factor leads to an increase of the phase noise.

6. Conclusions

In this article, an experimental online optimization of the flatness for optical frequency combs is demonstrated. By employing the differential evolution algorithm, a flatness of 2 dB is found for 7 carriers within the frequency comb. This is possible by driving a directly modulated laser with a signal composed of three harmonics with optimized amplitudes and phases provided by the optimization algorithm. The same methodology is also considered for a laser model. Therefore, only the laser is necessary and by shaping its driving signal a considerable number of lines within an optimal flatness can be achieved. The harmonic composition combined with the gradient-free algorithms proved to be an important asset for high-performance optical frequency combs design.

Funding. H2020 Marie Skłodowska-Curie Actions (814276; 754462); European Research Council (ERC-CoG FRECOM project grant agreement no. 771878); Science Fund of the Republic of Serbia (PROMIS, 6066816, iDUCOMBSENS); Ministarstvo Prosvete, Nauke i Tehnološkog Razvoja; Villum Fonden (VYI OPTIC-AI grant no. 29344).

Disclosures. The authors declare no conflicts of interest.

Data availability. Data underlying the results presented in this paper are not publicly available at this time but may be obtained from the authors upon reasonable request.

References

1. P. J. Delfyett, S. Gee, M.-T. Choi, H. Izadpanah, W. Lee, S. Ozharar, F. Quinlan, and T. Yilmaz, "Optical frequency combs from semiconductor lasers and applications in ultrawideband signal processing and communications," J. Lightwave Technol. **24**(7), 2701–2719 (2006).
2. P. Marin-Palomo, J. N. Kemal, T. J. Kippenberg, W. Freude, S. Randel, and C. Koos, "Performance of chip-scale optical frequency comb generators in coherent WDM communications," Opt. Express **28**(9), 12897–12910 (2020).
3. C. Browning, H. H. Elwan, E. P. Martin, S. O'Duill, J. Poette, P. Sheridan, A. Farhang, B. Cabon, and L. P. Barry, "Gain-switched optical frequency combs for future mobile radio-over-fiber millimeter-wave systems," J. Lightwave Technol. **36**(19), 4602–4610 (2018).
4. M. Mazur, A. Lorences-Riesgo, J. Schröder, P. A. Andrekson, and M. Karlsson, "10 Tb/s PM-64QAM self-homodyne comb-based superchannel transmission with 4% shared pilot tone overhead," J. Lightwave Technol. **36**(16), 3176–3184 (2018).
5. V. Torres-Company, J. Schröder, A. Fülöp, M. Mazur, L. Lundberg, Ó. Helgason, M. Karlsson, and P. A. Andrekson, "Laser frequency combs for coherent optical communications," J. Lightwave Technol. **37**(7), 1663–1670 (2019).
6. J. Kim and Y. Song, "Ultralow-noise mode-locked fiber lasers and frequency combs: principles, status, and applications," Adv. Opt. Photonics **8**(3), 465–540 (2016).
7. P. Lakshmijayasimha, A. Kaszubowska-Anandarajah, E. Martin, P. Landais, and P. Anandarajah, "Expansion and phase correlation of gain-switched optical frequency combs through FWM in an SOA," in *Proc. Opt. Fiber Commun. Conf.*, (IEEE, 2019), pp. 1–3.

Optics EXPRESS

8. W. T. Wang, J. G. Liu, W. H. Sun, W. Chen, and N. H. Zhu, "Multi-band local microwave signal generation based on an optical frequency comb generator," Opt. Commun. **338**, 90–94 (2015).
9. A. Parriaux, K. Hammani, and G. Millot, "Electro-optic frequency combs," Adv. Opt. Photonics **12**(1), 223–287 (2020).
10. A. Delmade, M. Krstić, C. Browning, J. Crnjanski, D. Gvozdić, and L. Barry, "Power efficient optical frequency comb generation using laser gain switching and dual-drive Mach-Zehnder modulator," Opt. Express **27**(17), 24135–24146 (2019).
11. R. Zhou, S. Latkowski, J. O'Carroll, R. Phelan, L. P. Barry, and P. Anandarajah, "40nm wavelength tunable gain-switched optical comb source," Opt. Express **19**(26), B415–B420 (2011).
12. A. Rosado, A. Pérez-Serrano, J. M. G. Tijero, Á. Valle, L. Pesquera, and I. Esquivias, "Experimental study of optical frequency comb generation in gain-switched semiconductor lasers," Opt. Laser Technol. **108**, 542–550 (2018).
13. Q. Wang, L. Huo, Y. Xing, and B. Zhou, "Ultra-flat optical frequency comb generator using a single-driven dual-parallel Mach–Zehnder modulator," Opt. Lett. **39**(10), 3050–3053 (2014).
14. G. F. Pendiuk, P. T. Neves, and A. A. Pohl, "Use of a differential evolution algorithm for determining input driving signals in optical frequency combs," OSA Continuum **3**(8), 2232–2242 (2020).
15. S. Ozharar, F. Quinlan, I. Ozdur, S. Gee, and P. Delfyett, "Ultraflat optical comb generation by phase-only modulation of continuous-wave light," IEEE Photonics. Tech. Lett. **20**(1), 36–38 (2008).
16. N. Yokota, K. Abe, S. Mieda, and H. Yasaka, "Harmonic superposition for tailored optical frequency comb generation by a Mach-Zehnder modulator," Opt. Lett. **41**(5), 1026–1029 (2016).
17. G. F. Pendiuk, P. T. Neves, and A. A. Pohl, "Flatness optimization of optical frequency combs using an adapted differential evolution algorithm," in *Frontiers in Optics*, (Optical Society of America, 2018), pp. JW3A–82.
18. A. Rosado, A. Pérez-Serrano, J. M. G. Tijero, Á. Valle, L. Pesquera, and I. Esquivias, "Numerical and experimental analysis of optical frequency comb generation in gain-switched semiconductor lasers," IEEE Journal of Quantum Electronics (2019).
19. Q. Bai, "Analysis of particle swarm optimization algorithm," CIS **3**(1), 180 (2010).
20. S. Koziel and X.-S. Yang, *Computational optimization, methods and algorithms*, vol. 356 (Springer, 2011).
21. T. Keating, X. Jin, S. L. Chuang, and K. Hess, "Temperature dependence of electrical and optical modulation responses of quantum-well lasers," IEEE J. Quantum Electron. **35**(10), 1526–1534 (1999).
22. L. A. Coldren, S. W. Corzine, and M. L. Mashanovitch, *Diode lasers and photonic integrated circuits*, vol. 218 (John Wiley & Sons, 2012).
23. Y. Zhang, S. Wang, and G. Ji, "A comprehensive survey on particle swarm optimization algorithm and its applications," Math. Probl. Eng. **2015**, 1–38 (2015).
24. J. Kennedy and R. Eberhart, "Particle swarm optimization," in *Proceedings of ICNN'95-international conference on neural networks*, vol. 4 (IEEE, 1995), pp. 1942–1948.